Environmental Science
Atmospheres

Accepted Manuscript

This article can be cited before page numbers have been issued, to do this please use: X. Zhang, Z. Chen, P. Zuo, Q. Liu and G. Jiang, *Environ. Sci.: Atmos.*, 2026, DOI: 10.1039/D6EA00052E.

ROYAL SOCIETY OF CHEMISTRY

rsc.li/esatmospheres

View Article Online
DOI: 10.1039/D6EA00052E

Environmental significance

$PM_{2.5}$ poses significant risks to human health, yet mechanistic studies are often limited by the complexity, variability, and scarcity of real ambient $PM_{2.5}$ samples. Existing $PM_{2.5}$ surrogates typically contain only a few components and fail to adequately represent the complexity of atmospheric particles. To address this challenge, we developed an easy and scalable spray-drying method for producing engineered $PM_{2.5}$ with controllable chemical compositions. The synthetic particles were designed to simulate key characteristics of real ambient $PM_{2.5}$, including particle size distribution, morphology, and elemental composition. Their environmental relevance was further evaluated through comparison with real $PM_{2.5}$ samples in terms of physicochemical properties and cytotoxicity. This innovation will empower researchers to conduct systematic investigations into component interactions, synergistic effects, and source-specific toxicity, thereby urgently advancing environmental health research and risk evaluation.

View Article Online
DOI: 10.1039/D6EA00052E

A one-step, scalable thermospray method for synthesis of multi-component particles mimicking atmospheric particulate matter

Xi-En Zhang[1,2], Zigu Chen[1], Peijie Zou[1,4], Qian Liu[1,3]*, Guibin Jiang[1,2,3]

[1] *State Key Laboratory of Environmental Chemistry and Toxicology, Research Center for Eco-Environmental Sciences, Beijing 100085, China*

[2] *School of Environment, Hangzhou Institute for Advanced Study, University of Chinese Academy of Sciences, Hangzhou 310024, China*

[3] *University of Chinese Academy of Sciences, Beijing 100190, China*

[4] *Institute of NBC Defense, PLA, Beijing 102205, China*

Email: qianliu@rcees.ac.cn

Abstract

The extremely high complexity in composition of $PM_{2.5}$ poses a major challenge in assessment of its environmental health risks. Laboratory-based toxicological studies are often limited by the scarcity of real environmental $PM_{2.5}$ samples, which are essential for various analyses. Most conventional sampling procedures yield insufficient amounts of $PM_{2.5}$ to meet the demands for physicochemical characterization, toxicological evaluation, and replication of findings. Current synthetic models typically consist of single or limited components, lacking the multi-component realism essential for accurate toxicity assessment. Here, we present a novel, facile, and scalable spray-drying method to fabricate multi-component model $PM_{2.5}$ particles with tunable chemical compositions, closely mimicking real ambient $PM_{2.5}$ in morphology, size distribution, and elemental profile. At the optimized temperature of 130 °C, over 70% of the synthesized particles were below 2.5 μm, with recovery rates of representative inorganic ions exceeding 97%. We also tested the biological toxicity response of these synthetic particles *in vitro*. This work provides a robust, reproducible, and accessible tool for particulate toxicology and broader airborne particle research to overcome critical supply and standardization barriers, thus enabling systematic investigation of component interactions, synergistic effects, and source-specific toxicity for advancing environmental health research and risk assessment of $PM_{2.5}$.

View Article Online
DOI: 10.1039/D6EA00052E

Keywords:

Fine particulate matter, thermospray, multi-component particle, synthesis, toxicology

Introduction

Air pollution is one of the leading global environmental risks to human health, contributing to more than six million premature deaths per year. As a major lethal part[1], ambient particulate matter (PM) accounted for 4.14 million deaths in 2019, and the populations exposed to PM pollution has steadily increased over the past 20 years[2, 3]. Specifically, fine particulate matter ($PM_{2.5}$) has been recognized as a major driver of adverse health effects, especially in the cardiovascular and respiratory systems[4, 5]. Although $PM_{2.5}$ poses a severe threat to public health, the key components responsible for its toxicity remain unclear due to the complexity and heterogeneity of its sources and compositions. Previous studies have variably attributed PM-induced cytotoxicity to heavy metals, inorganic components, or polycyclic aromatic hydrocarbons (PAHs), suggesting that the dominant toxic constituents may differ depending on PM sources and environmental conditions[6-8].

In most cases, $PM_{2.5}$ is a heterogeneous mixture consisting of inorganic components (e.g., transition metals, nitrate, sulfate, and carbon/silicon-based materials), organic components (e.g., volatile organic compounds and polycyclic aromatic hydrocarbons (PAHs)), and biogenic substances (e.g., bacteria, fungi, and viruses). Different origins of PM consist of various chemical species[9]. For example, volcanic ash contains plenty of inorganic salts, especially sulfate and metal oxides[10], while particles from biomass burning may contain high concentrations of PAHs and heavy metals[8, 11]. It should be noted that the composition of particulate matter can vary widely depending on the source, combustion conditions, and atmospheric processing, and the components mentioned here represent only a subset of the possible chemical species. Besides the differences caused by diverse emission sources, meteorological factors are also able to alter the contents of $PM_{2.5}$. In addition to variations caused by diverse emission sources, meteorological factors can influence $PM_{2.5}$ concentrations and composition. Consequently, the chemical composition of $PM_{2.5}$ exhibits significant spatial and temporal variability, not only across different regions and seasons, but also within individual cities and between day and night. These variations are driven by differences in local sources, atmospheric transport, chemical transformations, and diurnal meteorological patterns[12].

View Article Online
DOI: 10.1039/D6EA00052E

To elucidate the underlying toxicity mechanisms and associated health risks of $PM_{2.5}$, it is ideal to use real ambient $PM_{2.5}$ samples in experimental exposure studies. However, based on the literature and our experimental experience, obtaining sufficient quantities of authentic $PM_{2.5}$ samples for physicochemical analysis and *in vitro* or *in vivo* exposure experiments remains challenging[13]. Moreover, due to inherent variability arising from uncontrollable environmental parameters, real-world $PM_{2.5}$ samples collected via field sampling exhibit high inter-batch heterogeneity and irreproducibility, hindering the establishment of clear, consensus-based conclusions regarding key risk factors in disease pathogenesis. Thus, there is an imperative need to develop synthetic model $PM_{2.5}$ that enable a more precise and comprehensive understanding of $PM_{2.5}$-related toxicological responses and their possible triggers[14].

Recently, a reductionism approach has been proposed to elucidate key toxic factors, and carbon/silicon-based $PM_{2.5}$ libraries have been constructed to compare the relative toxicities of Pb, Cr, As, and benzo[a]pyrene (BaP)[15]. The chemical composition of model $PM_{2.5}$ can be adjusted according to scientific objectives. However, these models fail to fully represent real $PM_{2.5}$, because the number of components was limited, and common water-soluble ions and metal oxides were neglected[16]. Furthermore, the aqueous-phase synthetic conditions employed in these models deviate significantly from the physicochemical processes governing $PM_{2.5}$ formation in the atmosphere. Regarding synthesis of micro/nano-sized materials, a variety of methods are available, such as chemical precipitation[17-19], sol-gel[20, 21], freeze drying[22], and hydrothermal methods[23, 24]. However, the preparation conditions are usually restricted to liquid systems, which may not be suitable for $PM_{2.5}$ that contains water-insoluble components. Therefore, it is still challenging to develop strategies for mimicking PM particles.

Here we report a novel, rapid, easy thermospray-drying method for scalable synthesis of multi-component particles that mimic $PM_{2.5}$. The spray-drying methods have been successfully used in producing microsphere capsules, dehydrated food, metal-organic frameworks beads, and electrode materials[25-31]. While previous study employed a nebulizer–spray chamber system to generate aerosol particles for direct deposition onto cell cultures[16], the present spray-drying approach focuses on the scalable production and collection of $PM_{2.5}$ model particles. The method provides efficient particle recovery and enables optimization of both particle size distribution and chemical composition, thereby facilitating the preparation of reproducible $PM_{2.5}$ surrogate materials for laboratory-based exposure and toxicological investigations. In this method, raw ingredients

View Article Online
DOI: 10.1039/D6EA00052E

dissolved in solvent are sprayed in the nozzle and these processes the nuclei undergo are similar to the formation of $PM_{2.5}$ in the atmosphere[32]. The proposed spray-drying approach provides greater flexibility in incorporating multiple chemical components under relatively mild processing conditions. To evaluate the environmental relevance of the engineered particles, the synthesized $PM_{2.5}$ was systematically compared with real ambient $PM_{2.5}$ in terms of particle size distribution, elemental composition, and cytotoxicity.

Experimental section

Reagents

Sodium nitrate ($NaNO_3$), potassium nitrate (KNO_3), ammonium chloride (NH_4Cl), ammonium sulfate ($(NH_4)_2SO_4$), calcium nitrate ($Ca(NO_3)_2$), magnesium sulfate ($MgSO_4$), aluminum nitrate ($Al(NO_3)_3$), lead nitrate ($Pb(NO_3)_2$), zinc sulfate ($ZnSO_4$), lauric acid, terephthalic acid were purchased from Sinopharm Chemical Reagent (Beijing, China). Black carbon (BC), silicon dioxide (SiO_2), magnetite (Fe_3O_4), and Copper oxide (CuO) were nano-scale and bought from Sigma-Aldrich (Steinheim, Germany). Specific information, including product codes, specifications, and purity, is listed in Table S2. All reagents meet the purity requirements of analytical purity. MTT solution (0.5%) and ELISA assay for IL-6 were bought from Solarbio Life Science and Abbkine Scientific respectively.

Synthesis of model $PM_{2.5}$ samples

To establish a representative $PM_{2.5}$ formulation, research articles reporting $PM_{2.5}$ chemical composition in the Beijing region were collected from the Web of Science database using "Beijing" and "$PM_{2.5}$" as keywords. A total of 15 typical studies meeting the selection criteria were analyzed. The average mass fractions of the major components frequently reported in the literature were calculated and used as target composition values. Corresponding chemical standards were then selected and weighed according to these proportions to prepare the precursor suspension for subsequent spray-drying synthesis of engineered $PM_{2.5}$. All kinds of raw materials were weighted according to the determined prescription using an analytical balance (0.1 mg precision, Sartorius, Germany). Commercial Spray dryer device (B-290, BUCHI, Switzerland) was applied in this research to synthesize model particles and the main structures of the equipment included spray nozzle, cyclone separation system, and temperature-controlled drying system. The spray dryer equipped with a 0.7 mm two-fluid nozzle was used to synthesize engineered $PM_{2.5}$ particles. The

View Article Online
DOI: 10.1039/D6EA00052E

suspension, with 1% solid content, was delivered at a flow rate of 5 mL/min using a peristaltic pump. The inlet temperature of the drying gas was set to 130 ℃, while all other operating parameters were kept constant. Particles were separated from the drying gas stream using the instrument's proprietary high-efficiency collection vessel with a specialized coated surface and collected for further characterization. The temperature was set directly with the spray dryer on the instrument operation panel.

Collection of real $PM_{2.5}$ samples

The sample filters were cut into small pieces (1 cm^2) and extracted in 50 mL of ultra-pure water by sonication for 30 min. This step was repeated 4 times. After removal of the filters, the suspension was put in a vacuum desiccator to obtain $PM_{2.5}$ powders which were kept at -20 °C.

Characterization of morphology and elemental distribution

Approximately 0.1 g of the powder was weighed and evenly spread on weighing paper. Conductive tapes were attached to the carrier plate in advance, and the plate was positioned approximately 10 cm from the weighing paper. Nitrogen gas at a constant pressure of 0.1 MPa was used to disperse the powder, allowing $PM_{2.5}$ particles to fall freely onto the surface of the conductive tapes. Sizes, morphology, and elemental distributions of particles were measured with scanning electron microscopy (Quattro-ESEM, Thermo, USA) with a secondary electron detector and energy dispersive spectrometer (Element E1868, Ametek, USA). An accelerating voltage of 15 kV was used and signal acquisition mode was secondary electron. The results were counted and analyzed by ImageJ software automatically.

Ion Chromatography

The analysis of water-soluble anions followed the Chinese National Environmental Standard HJ 799-2016 ("*Determination of Water-Soluble Anions in Ambient Air Particulate Matter-Ion Chromatography Method*"). An ion chromatograph (ICS-2000, Dionex Integration) was used to analyze the concentrations of water-soluble anions, including Cl^-, SO_4^{2-}, and NO_3^-, using an AS15 separation column (44 × 250 mm, Dionex IonPac™), KOH eluent, injection volume 25 μL, column temperature = 30.0 °C, cell temperature = 35.0 °C, flow rate = 1.00 mL/min, runtime = 20 min.

Cell culture and $PM_{2.5}$ exposure

The human lung adenocarcinoma cell line A549 purchased from Cyagen Co. was maintained in DMEM medium in a 37 °C incubator in a mixed atmosphere containing 5% CO_2. The medium was changed every day, and trypsinized cells were passaged once in four days. $PM_{2.5}$ was dispersed

View Article Online
DOI: 10.1039/D6EA00052E

in a complete medium (DMEM culture medium, 5% FBS, 1% Penicillin, and Streptomycin) at a concentration of 1000 μg/mL as a stock solution. Before each pipetting step, the mixture is vortexed for 10 seconds to ensure that the dispersion remains uniform and stable. Then it was diluted to 10, 20, 40, 50, 80, 100, 160, and 200 μg/mL. A549 cells were implanted in 96-well microplates at a density of 1000 cells per well and incubated overnight. Afterward, the medium was replaced by the prepared solutions in sextuplicate. The operations of the control group were the same as the test group with the substitution of culture medium for $PM_{2.5}$. After 24 and 48 h of exposure, MTT and ELISA experiments were performed and the absorbance was quantified by using a VICTOR Nivo plate reader (Perkin Elmer, USA).

MTT experiments

$PM_{2.5}$ suspension at concentrations of 10, 20, 40, 50, 80, 100, 160, and 200 μg/mL were added into 96-well microplates, and cells were incubated after exposures for 24 and 48 h. Cell viability of A549 cells was tested with the MTT assay ([3-(4,5-dimethylthiazol-2-yl)-2,5-diphenyltetrazolium bromide]), for living cells were able to reduce exogenous MTT to water-insoluble blue-violet crystalline formazan and deposit it in the cell, whereas dead cells did not have such function. Specifically, 10 μL of MTT solution was added to each well, and incubated for 4 h at 37 °C after PM exposure, then 150 μL of dimethyl sulfoxide (DMSO) solution was added to each well, and the plate was plated on an oscillator and shaken for 10 min to dissolve all the formazan. The absorbances at 570 nm was measured with a microplate reader.

ELISA assays

$PM_{2.5}$ solutions at concentrations of 10, 50, and 200 μg/mL were added into 96-well microplates, and cells were incubated after exposures for 24 and 48 h. Then culture media were collected and centrifuged at 112×g to remove cell debris and suspended particles. All ELISA operations were conducted according to manufacturer instructions. The absorbance was measured at 450 nm within 30 minutes after the addition of the termination solution using an enzyme meter and 570 nm was set as the calibration wavelength. A standard curve was established based on absorbance and concentration of standards, and the concentration of each well was calculated.

Statistical analysis

All data were analyzed and presented as mean values ± standard deviation and all bar charts were exported by Graph-Pad Prism version 8.0.1 (GraphPad Software Inc., CA, USA). One-way ANOVA followed by LSD or Dunnett T3 post hoc tests were used to examine differences between

View Article Online
DOI: 10.1039/D6EA00052E

the average values of different groups. Statistical significance was defined as $*p < 0.05$.

Results and discussion

Determination of the ingredient lists

The inter-batch proportions of natural $PM_{2.5}$ components are highly variable, and thus there is no fixed formulation for synthesizing model $PM_{2.5}$. To establish a reliable concentration range of $PM_{2.5}$ components for subsequent experiments, relevant literature from the Beijing region over the past two decades was collected via Web of Science, and typical studies meeting the criteria were analyzed, with the data summarized in Table S1. It should be noted that $PM_{2.5}$ composition can vary across different regions worldwide due to differences in emission sources and environmental conditions. In this study, Beijing $PM_{2.5}$ was selected as the reference material because the primary objective was to validate the spray-drying method rather than to compare PM compositions globally. Nevertheless, the approach is flexible and can be adapted by researchers in other regions, who can adjust the precursor formulation according to the local $PM_{2.5}$ composition to generate region-specific engineered particles.

Common inorganic components such as sulfates, nitrates, chloride salts, cations, and metal oxide components were included and simulated by various chemicals Due to the complexity and diversity of organic compounds in ambient $PM_{2.5}$, it is impractical to represent all organic species in a single model formulation. Therefore, lauric acid and terephthalic acid were selected as representative organic compounds with distinct structural characteristics, namely long-chain aliphatic carbon backbones and aromatic benzene-ring structures, respectively. Lauric acid was chosen as a representative fatty acid because fatty acids are commonly detected in ambient particulate matter and are important constituents of cooking-related emissions[33-35], which can contribute substantially to human PM exposure. Terephthalic acid was selected as a representative aromatic organic compound because related benzene-ring-containing species and aromatic species are ubiquitous components of atmospheric $PM_{2.5}$ and are frequently associated with anthropogenic combustion sources[36, 37]. Together, these compounds provide a simplified representation of major structural classes of organic matter present in ambient $PM_{2.5}$, fatty acid and benzoate were chosen. In addition, silicon dioxide (SiO_2) as a non-metal component was added to the list because of its high abundance in $PM_{2.5}$ and important role in causing lung cancer[38]. According to the reference values in the literature, commercial reagents were weighed and detailed data are given in Table

View Article Online
DOI: 10.1039/D6EA00052E

S2.

Optimization of preparation conditions for model $PM_{2.5}$

In the spray-drying technology, parameters such as drying temperature, peristaltic pump flow rate, and percentage of solid content can affect the final sizes of products (Figure 1A). Notably, the particle size distribution of products was mainly determined by the temperature of drying gas. Other parameters were fixed based on preliminary experiments to ensure stable operation and reproducible particle production. During the preliminary trials, increasing the peristaltic pump feed rate resulted in the formation of dark sticky deposits around the nozzle, which was attributed to incomplete drying of the atomized droplets. In addition, increasing the solids content of the suspension led to severe deposition of nanoparticle powders in the beaker and the pipeline. These phenomena are consistent with previous reports indicating that excessive feed rates and high solids concentrations may promote incomplete drying, wall deposition, and nozzle fouling during spray drying[39, 40]. Therefore, peristaltic pump flow rate was set 5 mL/min and a solids content of 1% were selected for all subsequent experiments. These conditions minimized material deposition, ensured stable atomization, and improved the reproducibility of particle synthesis.

For aqueous solutions, the instrument's operating temperature range is from 100 °C to 200 °C. Since 150 °C is the most commonly used temperature in engineering applications, we have set this as the median value, with a temperature range of 50 °C, 130 °C and 180 °C serving as the lower and upper limits, respectively. The morphology and sizes of the synthesized particles at different temperatures are shown in Figure 1B-D, where temperatures were set at 130 °C, 150 °C, and 180 °C, respectively. The SEM images of the 130 ℃ synthesis products were analyzed by software; a total of 1822 particles meeting the requirements were highlighted in color and automatically counted (Figure 1B). Particle-size analysis of the thermos-sprayed products revealed that at 130 °C and 150 °C, approximately 70% and 68% of particles were below 2.5 μm, respectively, with over 98% smaller than 10 μm. At 180 °C, 54% of particles were below 2.5 μm, and 5% exceeded 10 μm. The mean particle diameters were ~2.23 μm, ~2.37 μm, and ~3.30 μm at 130 °C, 150 °C, and 180 °C, respectively. These results indicate that the thermos-spraying method effectively generates predominantly micron-sized particles, and that the particle-size distribution can be tuned by adjusting the temperature, demonstrating the suitability of this approach for preparing $PM_{2.5}$ model materials for subsequent toxicological studies.

The statistical results of particle size distribution are shown in Figure 1E and 1F. We found

View Article Online
DOI: 10.1039/D6EA00052E

that there was no significant difference between low (130 °C) and medium temperature (150 °C) groups. However, the high temperature (180 °C) group yielded distinctly different from the other two groups. At a higher temperature, more black paste-like material adhered around the nozzle, which appeared to be mixture of black carbon, iron oxide, or organic compounds. The possible reason may be that some substances such as organic chemicals are sensitive to high temperature and are easily agglomerated during the evaporation process, leading to an increase in the size of PM. In addition, high temperatures can accelerate solution evaporation, and substances (e.g., black carbon) with adsorption properties were more likely to merge and then aggregated into large particles.

Although higher temperature of the drying chamber led to a more rapid rate of solvent evaporation and PM nucleation, it may also cause low recovery of raw materials, because some volatile components may follow with the drying air stream out of the system and heat-sensitive reagents were easily lost because of adhesion to the nozzle; The phenomena are consistent with previous reports[41, 42]. In complex spray-drying systems, the retention of representative compounds is frequently used to evaluate component preservation when complete compositional analysis is impractical. Previous studies have employed the retention of main compounds and bioactive compounds as indicators of spray-drying performance[43, 44]. These ions were chosen because they constitute a substantial fraction of ambient $PM_{2.5}$, are chemically stable, and can be reliably quantified by ion chromatography, providing a practical proxy for evaluating material recovery. It should be noted that this approach reflects an approximate recovery of the total material and does not fully account for the organic fraction or other minor components. In this regard, the quantitative results of chloride, sulfate, and nitrate ions by ion chromatography were selected as indexes for evaluating the recovery rate of raw materials. The results are shown in Figure 2 and specific data of standard curves are given in Table S4. Results revealed that chloride ions were more sensitive to temperature than sulfate and nitrate ions (Figure 2A-C). For chloride ions, the maximum usage was 97.4% at 130 °C, which was almost three times higher than that at 150 °C (36.5%). The recovery rate rose slightly when the temperature increased to 180 °C. Nevertheless, it was still significantly lower than that at 130 °C (Figure 2A). A similar tendency in recovery was also observed in Figure 2B. Notably, nitrate ions showed the highest recovery efficiency at 130 °C, reaching 97.4%; the recovery rate decreased at 150 °C and subsequently increased slightly at 180 °C, which was consistent with the trend observed for chloride ions. For sulfate ions, the

View Article Online
DOI: 10.1039/D6EA00052E

synthetic efficiency was the lowest at 150 °C. Unlike chloride and nitrate ions, for sulfate ions, the performance at 180 °C was better than at 130 °C (Figure 2C), as the recovery rate was 71.8% and 86.8% at 130 °C and 180 °C, respectively. Accordingly, by modulating the parameters related to atomized droplet mass and the efficiency of heat transfer, an optimal balance was achieved was obtained to balance the diameters of PM and the recovery rate of reagents. Considering both the diameters and recovery rate, 130 °C was chosen as the optimal synthetic temperature.

Morphology characterization of synthetic $PM_{2.5}$

SEM and EDX were utilized to map elemental distribution at a 100 μm scale and conduct a semi-quantitative analysis of element content on a single particle scale. Figure S1 compares the spatial distribution of elements from $PM_{2.5}$ synthesized in the laboratory and samples collected in the real environment. Figure S1A shows spherical ferrous particles in the synthesized samples. According to the list of raw materials, it was likely that the spherical iron-containing particles were Fe_3O_4 particles. Fe_3O_4 was a common species in the atmosphere, which can be originated from various sources such as thermal power plants and brake pad wear[45]. Notably, similar results were also obtained with real $PM_{2.5}$ samples (Figure S1B). Besides metal oxides, SiO_2 particles were also detected in both spray-drying and real $PM_{2.5}$ (Figure S1C-D). These results implied that the elemental distribution was similar between the synthetic and real samples.

Figure 3A-D and Figure S2 indicate that chemical composition of synthetic $PM_{2.5}$ was largely dominated by nitrogen, oxygen, sulfur, and alkali metals, and few particles may consist of metals such as Fe, Cu, Zn, and Pb. The first image in Figure 3A is the raw electron microscope image; the remaining images are energy-dispersive X-ray spectroscopy maps. In the raw image, the gray bright spots represent particles, while the black background indicates the conductive adhesive. From a qualitative, visual perspective, it is evident that light elements largely coincide with the bright spots, whereas heavy elements are concentrated only in some of the gray bright spots, indicating a heterogeneous distribution. Furthermore, elements with higher solubility and greater abundance were more homogeneously distributed, while those with lower content and lower solubility in the $PM_{2.5}$ showed more heterogeneous distributions. This phenomenon was also similar to the elemental distribution patterns of natural $PM_{2.5}$. This may be because sulfate and nitrate salts could be recrystallized during spray drying to generate a homogeneous redistribution. We hypothesize that the relatively homogeneous distribution of sulfate- and nitrate-containing species may be associated with recrystallization or phase redistribution processes during spray

View Article Online
DOI: 10.1039/D6EA00052E

drying, as internal component redistribution during recrystallization have been reported in inorganic aerosol[46]. However, further investigations are required to confirm the underlying mechanism in the present system.

Taking Figure 3C as an example, the distribution characteristics and correlations among the various elements are quantitatively analyzed. Spearman correlation analysis was performed on elements from typical SEM-EDX results using Python and imageJ coloc 2. The heat map and PCA results of elements (Figure 3F-H) also show that light elements within the synthetic $PM_{2.5}$ samples such as N, O, Na, K, and S exhibited homogeneous distribution. Conversely, heavier elements such as Fe, Cu, Zn, and Pb demonstrated heterogeneous distributions, being localized to specific regions within particles rather than uniformly dispersed. Correlation analysis of element distribution indicated that the coefficients for Pb and Cu-Zn exceed 0.4, which was significantly higher than those for other light elements, implying their close spatial proximity. Previous research has reported that metallic components, such as Fe, Pb, and Zn, frequently cluster together in $PM_{2.5}$ emitted from coal combustion[47, 48]. The elemental distribution patterns of as-prepared particles aligned with those observed in real $PM_{2.5}$. Furthermore, previous studies have revealed that secondary aerosols, containing components such as sulfate and nitrate, can contribute over 40% of the $PM_{2.5}$ mass[49, 50]. The secondary formation reaction is widespread and readily combines with alkali metals such as Na, K, and Ca. This observation was consistent with our findings in this study. PCA loading scores indicated that both acidic elements and alkali metal cations exhibited a synchronous downward trend, suggesting that their distribution patterns remained fundamentally consistent.

Cytotoxicity of synthetic $PM_{2.5}$ with A549 cells

Exposure to $PM_{2.5}$ can induce oxidative stress and inflammatory responses in organisms, leading to systemic health risks. Following the aforementioned experiments, we further tested the cytotoxicity of the synthetic $PM_{2.5}$. Given that respiratory exposure is the main route of $PM_{2.5}$ exposure, human lung-derived A549 cells were selected as the cellular model for this study. To investigate cytotoxic effects, the inflammatory response, specifically the secretion of interleukin 6 (IL-6) was evaluated. Meanwhile, the MTT assay was conducted to assess cell viability after exposure to $PM_{2.5}$. Cell viability data following $PM_{2.5}$ exposure are presented in Figure 4. These results showed a significant reduction in A549 cell viability in the exposed group compared to the control group, probably due to $PM_{2.5}$ exposure generating reactive oxygen species (ROS) and

View Article Online
DOI: 10.1039/D6EA00052E

inducing homeostatic disorder, ultimately causing cell dysfunction and death. Detailed percentages of viable cells exposed to various $PM_{2.5}$ concentrations (10-200 μg/mL) are given in Table S3. After 24 h of incubation, the highest inhibition rate reached 31.1%. Within the concentration range of 40 to 200 μg/mL, the inhibition rate remained at ~30% with slight fluctuations, and these differences were statistically significant compared to the control group (Figure 4A). At the incubation time of 48 h, a similar trend was observed (Figure 4B).

Previous studies have repeatedly validated the dose- and time-dependent relationships of cell viability and cytokines with $PM_{2.5}$ samples across different countries and seasons[51-54]. We also observed that the IL-6 concentration exhibited time- and dose-dependent relationships (Figure 4C). Generally, IL-6 concentrations were elevated in all exposed groups compared to the control group, suggesting that exposure to synthetic $PM_{2.5}$ particles induced a cellular inflammatory response. Considering the great variations in the toxicity of $PM_{2.5}$, here we did not directly compare the cytotoxicity between synthetic and real $PM_{2.5}$.

Conclusion

This research may offer significant contributions to the field of particulate matter toxicology. The extreme heterogeneity and variability of ambient $PM_{2.5}$ pose a persistent challenge for reproducible toxicological studies. The inability to consistently obtain sufficient quantities of real-world $PM_{2.5}$ samples has historically hindered a deep understanding of their specific components and interactions driving adverse health effects. Our development of a facile and scalable spray-drying method to synthesize multi-component model $PM_{2.5}$ particles with tunable compositions directly addresses this major bottleneck. These synthetic particles closely mimic real ambient $PM_{2.5}$ in morphology, size, and elemental profile. This advancement provides a robust, standardized, and accessible tool that empowers researchers to systematically investigate the toxicological impact of specific particle components, their synergistic effects, and source-specific toxicity. Such progress is essential for developing more accurate environmental health risk assessments and informing targeted pollution control strategies.

At the same time, this work has inherent limitations. Firstly, although the synthetic particles mimic real $PM_{2.5}$ in morphology and elemental composition, they are still simplified models that may not fully capture the complete spectrum of chemical species present in ambient particles, especially complex organic fractions and biological components (e.g., bacteria, fungi). Secondly,

View Article Online
DOI: 10.1039/D6EA00052E

while *in vitro* toxicity responses are validated, direct *in vivo* extrapolation and confirmation of these findings would further strengthen the physiological relevance. Lastly, the current study focused on a representative set of components; further exploration of a wider range of chemical compositions and their combinations would be beneficial for broader applicability across different geographical regions and emission sources.

Supporting Information

The Supporting Information is available free of charge online.

Notes

The authors declare no competing financial interest.

Acknowledgment

This work was financially supported by the National Key R&D Program of China (2023YFC3708302), National Natural Science Foundation of China (No. 22425041, 22188102, 22193050, and 22576215), and Chinese Academy of Sciences Project for Young Scientists in Basic Research (YSBR-086).

References:

1. Beelen, R.; Raaschou-Nielsen, O.; Stafoggia, M.; Andersen, Z. J.; Weinmayr, G.; Hoffmann, B.; Wolf, K.; Samoli, E.; Fischer, P.; Nieuwenhuijsen, M.; Vineis, P.; Xun, W. W.; Katsouyanni, K.; Dimakopoulou, K.; Oudin, A.; Forsberg, B.; Modig, L.; Havulinna, A. S.; Lanki, T.; Turunen, A.; Oftedal, B.; Nystad, W.; Nafstad, P.; De Faire, U.; Pedersen, N. L.; Östenson, C.-G.; Fratiglioni, L.; Penell, J.; Korek, M.; Pershagen, G.; Eriksen, K. T.; Overvad, K.; Ellermann, T.; Eeftens, M.; Peeters, P. H.; Meliefste, K.; Wang, M.; Bueno-de-Mesquita, B.; Sugiri, D.; Krämer, U.; Heinrich, J.; de Hoogh, K.; Key, T.; Peters, A.; Hampel, R.; Concin, H.; Nagel, G.; Ineichen, A.; Schaffner, E.; Probst-Hensch, N.; Künzli, N.; Schindler, C.; Schikowski, T.; Adam, M.; Phuleria, H.; Vilier, A.; Clavel-Chapelon, F.; Declercq, C.; Grioni, S.; Krogh, V.; Tsai, M.-Y.; Ricceri, F.; Sacerdote, C.; Galassi, C.; Migliore, E.; Ranzi, A.; Cesaroni, G.; Badaloni, C.; Forastiere, F.; Tamayo, I.; Amiano, P.; Dorronsoro, M.; Katsoulis, M.; Trichopoulou, A.; Brunekreef, B.; Hoek, G., Effects of long-term exposure to air pollution on natural-cause mortality: an analysis of 22 European cohorts within the multicentre ESCAPE project. *The Lancet* **2014,** *383*, (9919), 785-795.
2. GBD 2020 Causes of Death Collaborators., Global burden of 87 risk factors in 204 countries and territories, 1990–2019: a systematic analysis for the Global Burden of Disease Study 2019. *The Lancet* **2020,** *396*, (10258), 1223-1249.

View Article Online
DOI: 10.1039/D6EA00052E

3. GBD 2023 Causes of Death Collaborators, Global burden of 292 causes of death in 204 countries and territories and 660 subnational locations, 1990–2023:a systematic analysis for the Global Burden of Disease Study 2023. *The Lancet* **2025**, 406, (10513), 1811-1872.
4. Hystad, P.; Larkin, A.; Rangarajan, S.; AlHabib, K. F.; Avezum, Á.; Calik, K. B. T.; Chifamba, J.; Dans, A.; Diaz, R.; du Plessis, J. L.; Gupta, R.; Iqbal, R.; Khatib, R.; Kelishadi, R.; Lanas, F.; Liu, Z.; Lopez-Jaramillo, P.; Nair, S.; Poirier, P.; Rahman, O.; Rosengren, A.; Swidan, H.; Tse, L. A.; Wei, L.; Wielgosz, A.; Yeates, K.; Yusoff, K.; Zatoński, T.; Burnett, R.; Yusuf, S.; Brauer, M., Associations of outdoor fine particulate air pollution and cardiovascular disease in 157 436 individuals from 21 high-income, middle-income, and low-income countries (PURE): a prospective cohort study. *The Lancet Planetary Health* **2020,** *4*, (6), e235-e245.
5. Guan, W.-J.; Zheng, X.-Y.; Chung, K. F.; Zhong, N.-S., Impact of air pollution on the burden of chronic respiratory diseases in China: time for urgent action. *The Lancet* **2016,** *388*, (10054), 1939-1951.
6. Yuan, Y.; Wu, Y.; Ge, X.; Nie, D.; Wang, M.; Zhou, H.; Chen, M., In vitro toxicity evaluation of heavy metals in urban air particulate matter on human lung epithelial cells. *Science of The Total Environment* **2019,** *678*, 301-308.
7. Perrone, M. G.; Gualtieri, M.; Ferrero, L.; Porto, C. L.; Udisti, R.; Bolzacchini, E.; Camatini, M., Seasonal variations in chemical composition and in vitro biological effects of fine PM from Milan. *Chemosphere* **2010,** *78*, (11), 1368-1377.
8. Yang, M.; Zeng, H.-X.; Wang, X.-F.; Hakkarainen, H.; Leskinen, A.; Komppula, M.; Roponen, M.; Wu, Q.-Z.; Xu, S.-L.; Lin, L.-Z.; Liu, R.-Q.; Hu, L.-W.; Yang, B.-Y.; Zeng, X.-W.; Dong, G.-H.; Jalava, P., Sources, chemical components, and toxicological responses of size segregated urban air PM samples in high air pollution season in Guangzhou, China. *Science of The Total Environment* **2023,** *865*, 161092.
9. Moreno-Ríos, A. L.; Tejeda-Benítez, L. P.; Bustillo-Lecompte, C. F., Sources, characteristics, toxicity, and control of ultrafine particles: An overview. *Geoscience Frontiers* **2022,** *13*, (1), 101147.
10. Tomašek, I.; Damby, D. E.; Stewart, C.; Horwell, C. J.; Plumlee, G.; Ottley, C. J.; Delmelle, P.; Morman, S.; El Yazidi, S.; Claeys, P.; Kervyn, M.; Elskens, M.; Leermakers, M., Development of a simulated lung fluid leaching method to assess the release of potentially toxic elements from volcanic ash. *Chemosphere* **2021,** *278*, 130303.
11. Etchie, A. T.; Etchie, T. O.; Elemile, O. O.; Boladale, O.; Oni, T.; Akanno, I.; Bankole, D. T.; Ibitoye, O. O.; Pillarisetti, A.; Sivanesan, S.; Afolabi, T. Y.; Krishnamurthi, K.; Swaminathan, N., Burn to kill: Wood ash a silent killer in Africa. *Science of The Total Environment* **2020,** *748*, 141316.
12. Gao, Z.; Ivey, C. E.; Blanchard, C. L.; Do, K.; Lee, S.-M.; Russell, A. G., Emissions, meteorological and climate impacts on PM2.5 levels in Southern California using a generalized additive model: Historic trends and future estimates. *Chemosphere* **2023,** *325*, 138385.
13. Kumar, P.; Kalaiarasan, G.; Porter, A. E.; Pinna, A.; Kłosowski, M. M.; Demokritou, P.; Chung, K. F.; Pain, C.; Arvind, D. K.; Arcucci, R.; Adcock, I. M.; Dilliway, C., An overview of methods of fine and ultrafine particle collection for physicochemical characterisation and toxicity assessments. *Science of The Total Environment* **2021,** *756*.
14. Pan, X.; Yu, Q.; Chen, S.; Li, Y.; Jiao, T.; Li, W.; Zhang, C.; Kureshi, A.; Cheng, L.; Xu, Q., Dissecting contributions of representative heavy metal components in PM2.5 to its cytotoxicity. *Ecotoxicology and Environmental Safety* **2023,** *251*, 143553.
15. Liu, G.; Yan, X.; Wang, S.; Yu, Q.; Jia, J.; Yan, B., Elucidation of the Critical Role of Core

View Article Online
DOI: 10.1039/D6EA00052E

Materials in PM2.5-Induced Cytotoxicity by Interrogating Silica- and Carbon-Based Model PM2.5 Particle Libraries. *Environmental Science & Technology* **2021,** *55*, (9), 6128-6139.
16. Fenwick, S.; Agnes, G. R., Nebulizer-spray chamber apparatus and method for production of multi-component particle types and their use in affecting cellular responses. *Aerosol Science and Technology* **2016,** *50*, (12), 1397-1409.
17. Sahai, A.; Goswami, N., Structural and vibrational properties of ZnO nanoparticles synthesized by the chemical precipitation method. *Physica E: Low-dimensional Systems and Nanostructures* **2014,** *58*, 130-137.
18. Syam Sundar, L.; Singh, M. K.; Ferro, M. C.; Sousa, A. C. M., Experimental investigation of the thermal transport properties of graphene oxide/Co 3 O 4 hybrid nanofluids. *International Communications in Heat and Mass Transfer* **2017,** *84*, 1-10.
19. Ambrus, Z.; Balázs, N.; Alapi, T.; Wittmann, G.; Sipos, P.; Dombi, A.; Mogyorósi, K., Synthesis, structure and photocatalytic properties of Fe(III)-doped TiO2 prepared from TiCl3. *Applied Catalysis B: Environmental* **2008,** *81*, (1-2), 27-37.
20. Parashar, M.; Shukla, V. K.; Singh, R., Metal oxides nanoparticles via sol–gel method: a review on synthesis, characterization and applications. *Journal of Materials Science: Materials in Electronics* **2020,** *31*, (5), 3729-3749.
21. Bokov, D.; Turki Jalil, A.; Chupradit, S.; Suksatan, W.; Javed Ansari, M.; Shewael, I. H.; Valiev, G. H.; Kianfar, E.; Wang, Z., Nanomaterial by Sol-Gel Method: Synthesis and Application. *Advances in Materials Science and Engineering* **2021,** *2021*, 1-21.
22. Bescond, A.; Oster, C.; Fisicaro, P.; Goddard, S.; Quincey, P.; Tsakanika, L.-A.; Lymperopoulou, T.; Ochsenkuehn-Petropoulou, M., Method for Preparation of a Candidate Reference Material of PM10 and PM2.5 Airborne Particulate Filters Loaded with Incineration Ash-Inter Comparison Results for Metal Concentrations. *Atmosphere* **2021,** *12*, (1), 67.
23. Agarwal, S.; Rai, P.; Gatell, E. N.; Llobet, E.; Güell, F.; Kumar, M.; Awasthi, K., Gas sensing properties of ZnO nanostructures (flowers/rods) synthesized by hydrothermal method. *Sensors and Actuators B: Chemical* **2019,** *292*, 24-31.
24. Liang, H.; Sun, R.; Song, B.; Sun, Q.; Peng, P.; She, D., Preparation of nitrogen-doped porous carbon material by a hydrothermal-activation two-step method and its high-efficiency adsorption of Cr(VI). *Journal of Hazardous Materials* **2020,** *387*, 121987.
25. Wu, J.; Andrews, M. P., Mechanical, morphological and comparative properties of microbeads assembled from carboxylated cellulose nanocrystals. *Journal of Materials Chemistry A* **2024,** *12*, (2), 950-960.
26. Di Giorgio, L.; Salgado, P. R.; Mauri, A. N., Nanocomposite systems based on soy proteins and cellulose nanocrystals to encapsulate fish oil by emulsification and spray-drying. *Cellulose* **2023,** *30*, (17), 10971-10982.
27. Liu, M.; Li, H.; Yu, J.; Zhang, S.; Chen, Q.; Lu, W.; Yuan, A.; Zhong, L.; Sun, L., Hierarchical structure promoted lithiation/delithiation behavior of a double-carbon microsphere supported nano-Co3O4 anode. *Nanoscale* **2024,** *16*, (6), 3043-3052.
28. Na, J. H.; Oh, H. G.; Lee, S.; Park, S.-K., Designing a 3D MXene microsphere encapsulating MOF-derived ZnSe nanoparticles as an anode for highly stable potassium-ion batteries. *Journal of Materials Chemistry A* **2024,** *12*, (5), 2848-2855.
29. Garzón-Tovar, L.; Rodríguez-Hermida, S.; Imaz, I.; Maspoch, D., Spray Drying for Making Covalent Chemistry: Postsynthetic Modification of Metal–Organic Frameworks. *Journal of the American Chemical Society* **2017,** *139*, (2), 897-903.
30. Liu, J.; Wei, Y.; Chang, M.; Wang, N.; Wang, D.; Wang, J. X., Rapid construction of

View Article Online
DOI: 10.1039/D6EA00052E

hierarchically porous metal–organic frameworks by a spray-drying strategy for enhanced tannic acid adsorption. *AIChE Journal* **2021,** *68*, (2), e17522.
31. Boix, G.; Troyano, J.; Garzón-Tovar, L.; Camur, C.; Bermejo, N.; Yazdi, A.; Piella, J.; Bastus, N. G.; Puntes, V. F.; Imaz, I.; Maspoch, D., MOF-Beads Containing Inorganic Nanoparticles for the Simultaneous Removal of Multiple Heavy Metals from Water. *ACS Applied Materials & Interfaces* **2020,** *12*, (9), 10554-10562.
32. Shang, D.; Peng, J.; Guo, S.; Wu, Z.; Hu, M., Secondary aerosol formation in winter haze over the Beijing-Tianjin-Hebei Region, China. *Frontiers of Environmental Science & Engineering* **2020,** *15*, (2), 34.
33. Zhou, W.; Zhao, Y.; Li, R.; Fu, H.; Li, Q.; Zhang, L.; Chen, J., Metals, PAHs and oxidative potential of size-segregated particulate matter and inhalational carcinogenic risk of cooking at a typical university canteen in Shanghai, China. *Atmospheric Environment* **2022,** *287*, 119250.
34. Guo, Z.; Chen, X.; Wu, D.; Huo, Y.; Cheng, A.; Liu, Y.; Li, Q.; Chen, J., Higher Toxicity of Gaseous Organics Relative to Particulate Matters Emitted from Typical Cooking Processes. *Environmental Science & Technology* **2023,** *57*, (44), 17022-17031.
35. Sankhyan, S.; Zabinski, K.; O'Brien, R. E.; Coyan, S.; Patel, S.; Vance, M. E., Aerosol emissions and their volatility from heating different cooking oils at multiple temperatures. *Environmental Science: Atmospheres* **2022,** *2*, (6), 1364-1375.
36. Alang, A. K.; Aggarwal, S. G.; Johri, P.; Hegde, P., Characterization, sources, and formation processes of dicarboxylic acids, oxocarboxylic acids and α-dicarbonyls in PM2.5 aerosols in New Delhi. *Atmospheric Environment* **2024,** *336*, 120759.
37. Liu, D.; Xu, S.; Lang, Y.; Hou, S.; Wei, L.; Pan, X.; Sun, Y.; Wang, Z.; Kawamura, K.; Fu, P., Seasonal variation and size distribution of aromatic acids in urban aerosols in Beijing, China. *Science of The Total Environment* **2024,** *954*, 176504.
38. Hill, W.; Lim, E. L.; Weeden, C. E.; Lee, C.; Augustine, M.; Chen, K.; Kuan, F.-C.; Marongiu, F.; Evans, E. J.; Moore, D. A.; Rodrigues, F. S.; Pich, O.; Bakker, B.; Cha, H.; Myers, R.; van Maldegem, F.; Boumelha, J.; Veeriah, S.; Rowan, A.; Naceur-Lombardelli, C.; Karasaki, T.; Sivakumar, M.; De, S.; Caswell, D. R.; Nagano, A.; Black, J. R. M.; Martínez-Ruiz, C.; Ryu, M. H.; Huff, R. D.; Li, S.; Favé, M.-J.; Magness, A.; Suárez-Bonnet, A.; Priestnall, S. L.; Lüchtenborg, M.; Lavelle, K.; Pethick, J.; Hardy, S.; McRonald, F. E.; Lin, M.-H.; Troccoli, C. I.; Ghosh, M.; Miller, Y. E.; Merrick, D. T.; Keith, R. L.; Al Bakir, M.; Bailey, C.; Hill, M. S.; Saal, L. H.; Chen, Y.; George, A. M.; Abbosh, C.; Kanu, N.; Lee, S.-H.; McGranahan, N.; Berg, C. D.; Sasieni, P.; Houlston, R.; Turnbull, C.; Lam, S.; Awadalla, P.; Grönroos, E.; Downward, J.; Jacks, T.; Carlsten, C.; Malanchi, I.; Hackshaw, A.; Litchfield, K.; Lester, J. F.; Bajaj, A.; Nakas, A.; Sodha-Ramdeen, A.; Ang, K.; Tufail, M.; Chowdhry, M. F.; Scotland, M.; Boyles, R.; Rathinam, S.; Wilson, C.; Marrone, D.; Dulloo, S.; Fennell, D. A.; Matharu, G.; Shaw, J. A.; Riley, J.; Primrose, L.; Boleti, E.; Cheyne, H.; Khalil, M.; Richardson, S.; Cruickshank, T.; Price, G.; Kerr, K. M.; Benafif, S.; Gilbert, K.; Naidu, B.; Patel, A. J.; Osman, A.; Lacson, C.; Langman, G.; Shackleford, H.; Djearaman, M.; Kadiri, S.; Middleton, G.; Leek, A.; Hodgkinson, J. D.; Totten, N.; Montero, A.; Smith, E.; Fontaine, E.; Granato, F.; Doran, H.; Novasio, J.; Rammohan, K.; Joseph, L.; Bishop, P.; Shah, R.; Moss, S.; Joshi, V.; Crosbie, P.; Gomes, F.; Brown, K.; Carter, M.; Chaturvedi, A.; Priest, L.; Oliveira, P.; Lindsay, C. R.; Blackhall, F. H.; Krebs, M. G.; Summers, Y.; Clipson, A.; Tugwood, J.; Kerr, A.; Rothwell, D. G.; Kilgour, E.; Dive, C.; Aerts, H. J. W. L.; Schwarz, R. F.; Kaufmann, T. L.; Wilson, G. A.; Rosenthal, R.; Van Loo, P.; Birkbak, N. J.; Szallasi, Z.; Kisistok, J.; Sokac, M.; Salgado, R.; Diossy, M.; Demeulemeester, J.; Bunkum, A.; Stewart, A.; Frankell, A. M.; Karamani, A.; Toncheva, A.;

View Article Online
DOI: 10.1039/D6EA00052E

Huebner, A.; Chain, B.; Campbell, B. B.; Castignani, C.; Puttick, C.; Richard, C.; Hiley, C. T.; Pearce, D. R.; Karagianni, D.; Biswas, D.; Levi, D.; Hoxha, E.; Cadieux, E. L.; Colliver, E.; Nye, E.; Gálvez-Cancino, F.; Athanasopoulou, F.; Gimeno-Valiente, F.; Kassiotis, G.; Stavrou, G.; Mastrokalos, G.; Zhai, H.; Lowe, H. L.; Matos, I. G.; Goldman, J.; Reading, J. L.; Herrero, J.; Rane, J. K.; Nicod, J.; Lam, J. M.; Hartley, J. A.; Peggs, K. S.; Enfield, K. S. S.; Selvaraju, K.; Thol, K.; Ng, K. W.; Dijkstra, K.; Grigoriadis, K.; Thakkar, K.; Ensell, L.; Shah, M.; Duran, M. V.; Litovchenko, M.; Sunderland, M. W.; Dietzen, M.; Leung, M.; Escudero, M.; Angelova, M.; Tanić, M.; Chervova, O.; Lucas, O.; Al-Sawaf, O.; Prymas, P.; Hobson, P.; Pawlik, P.; Stone, R. K.; Bentham, R.; Hynds, R. E.; Vendramin, R.; Saghafinia, S.; López, S.; Gamble, S.; Ung, S. K. A.; Quezada, S. A.; Vanloo, S.; Zaccaria, S.; Hessey, S.; Ward, S.; Boeing, S.; Beck, S.; Bola, S. K.; Denner, T.; Marafioti, T.; Mourikis, T. P.; Watkins, T. B. K.; Spanswick, V.; Barbè, V.; Lu, W.-T.; Liu, W. K.; Wu, Y.; Naito, Y.; Ramsden, Z.; Veiga, C.; Royle, G.; Collins-Fekete, C.-A.; Fraioli, F.; Ashford, P.; Clark, T.; Forster, M. D.; Lee, S. M.; Borg, E.; Falzon, M.; Papadatos-Pastos, D.; Wilson, J.; Ahmad, T.; Procter, A. J.; Ahmed, A.; Taylor, M. N.; Nair, A.; Lawrence, D.; Patrini, D.; Navani, N.; Thakrar, R. M.; Janes, S. M.; Hoogenboom, E. M.; Monk, F.; Holding, J. W.; Choudhary, J.; Bhakhri, K.; Scarci, M.; Hayward, M.; Panagiotopoulos, N.; Gorman, P.; Khiroya, R.; Stephens, R. C. M.; Wong, Y. N. S.; Bandula, S.; Sharp, A.; Smith, S.; Gower, N.; Dhanda, H. K.; Chan, K.; Pilotti, C.; Leslie, R.; Grapa, A.; Zhang, H.; AbdulJabbar, K.; Pan, X.; Yuan, Y.; Chuter, D.; MacKenzie, M.; Chee, S.; Alzetani, A.; Cave, J.; Scarlett, L.; Richards, J.; Ingram, P.; Austin, S.; Lim, E.; De Sousa, P.; Jordan, S.; Rice, A.; Raubenheimer, H.; Bhayani, H.; Ambrose, L.; Devaraj, A.; Chavan, H.; Begum, S.; Buderi, S. I.; Kaniu, D.; Malima, M.; Booth, S.; Nicholson, A. G.; Fernandes, N.; Shah, P.; Proli, C.; Hewish, M.; Danson, S.; Shackcloth, M. J.; Robinson, L.; Russell, P.; Blyth, K. G.; Dick, C.; Le Quesne, J.; Kirk, A.; Asif, M.; Bilancia, R.; Kostoulas, N.; Thomas, M.; DeGregori, J.; Jamal-Hanjani, M.; Swanton, C., Lung adenocarcinoma promotion by air pollutants. *Nature* **2023,** *616*, (7955), 159-167.
39. Keshani, S.; Daud, W. R. W.; Nourouzi, M. M.; Namvar, F.; Ghasemi, M., Spray drying: An overview on wall deposition, process and modeling. *Journal of Food Engineering* **2015,** *146*, 152-162.
40. Lechanteur, A.; Evrard, B., Influence of Composition and Spray-Drying Process Parameters on Carrier-Free DPI Properties and Behaviors in the Lung: A review. *Pharmaceutics* **2020,** *12*, (1), 55.
41. Mark, R. E.; Judeon K., Loss of Volatile Trace Organics during Spray Drying. *Industrial & Engineering Chemistry Process Design and Development* **1984,** *23*, 705-710.
42. Judson King, C., Spray Drying: Retention of Volatile Compounds Revisited. *Drying Technology* **2007,** *13*, (5-7), 1221-1240.
43. William, E. B.; Reineccius, G. A., Influence of Dryer lnfeed Matrices on the Retention of Volatile Flavor Compounds During Spray Drying. *Journal OF Food Science* **1981**,*47*,254-259.
44. Gimbun, J.; Nguang, S. L.; Pang, S. F.; Yeong, Y. L.; Kee, K. L.; Chin, S. C., Assessment of Phenolic Compounds Stability and Retention during Spray Drying of Phyllanthus niruri Extracts. *Industrial & Engineering Chemistry Research* **2018,** *58*, (2), 752-761.
45. Liu, L.; Zhang, Q.; Gui, J.; Zhang, B.; Yang, H.; Lu, D.; Chen, Z.; Liu, Q.; Li, Z.; Jiang, G., Traffic-derived magnetite pollution in soils along a highway on the Tibetan Plateau. *Environmental Science: Nano* **2022,** *9*, (2), 621-631.
46. Davis, R. D.; Lance, S.; Gordon, J. A.; Ushijima, S. B.; Tolbert, M. A., Contact efflorescence as a pathway for crystallization of atmospherically relevant particles. *Proceedings*

View Article Online
DOI: 10.1039/D6EA00052E

of the National Academy of Sciences **2015,** *112*, (52), 15815-15820.
47. Zhang, Y.; Zhang, J.; Jiang, X.; Wang, Y.; Ding, X.; Li, W., PM2.5-bound metallic elements in village and urban airs in North China during wintertime: Concentration, morphology, mixing state, and size distribution. *Journal of Environmental Sciences* **2025,** *158*, 724-734.
48. Li, W.; Shao, L., Transmission electron microscopy study of aerosol particles from the brown hazes in northern China. *Journal of Geophysical Research: Atmospheres* **2009,** *114*, (D9), D09302.
49. Zhang, J.; Sun, W.; Su, Y.; Peng, X.; Chen, C.; Fu, X.; Long, Y.; Wang, G.; Rao, Z.; Han, L.; Huang, X., Chemical composition, sources, and processes of winter haze in Chengdu, China: Insights from integrating the bulk chemical and single particle approaches. *Atmospheric Environment* **2024,** *322*, 120371.
50. Fakhri, N.; Stevens, R.; Downey, A.; Oikonomou, K.; Sciare, J.; Afif, C.; Hayes, P. L., Source apportionment of PM2.5 in Montréal, Canada, and health risk assessment for potentially toxic elements. *Atmospheric Chemistry and Physics* **2024,** *24*, (2), 1193-1212.
51. Xia, Y.; Zhang, X.; Sun, D.; Gao, Y.; Zhang, X.; Wang, L.; Cai, Q.; Wang, Q.; Sun, J., Effects of water-soluble components of atmospheric particulates from rare earth mining areas in China on lung cancer cell cycle. *Particle and Fibre Toxicology* **2021,** *18*, (1), 27.
52. Rahmatinia, T.; Kermani, M.; Farzadkia, M.; Jonidi Jafari, A.; Delbandi, A.-A.; Rashidi, N.; Fanaei, F., The effect of PM2.5-related hazards on biomarkers of bronchial epithelial cells (A549) inflammation in Karaj and Fardis cities. *Environmental Science and Pollution Research* **2021,** *29*, (2), 2172-2182.
53. Dou, C.; Zhang, J.; Qi, C., Cooking oil fume-derived PM2.5 induces apoptosis in A549 cells and MAPK/NF-κB/STAT1 pathway activation. *Environmental Science and Pollution Research* **2018,** *25*, (10), 9940-9948.
54. Huang, M.; Kang, Y.; Wang, W.; Chan, C. Y.; Wang, X.; Wong, M. H., Potential cytotoxicity of water-soluble fraction of dust and particulate matters and relation to metal(loid)s based on three human cell lines. *Chemosphere* **2015,** *135*, 61-66.

View Article Online
DOI: 10.1039/D6EA00052E

Figures

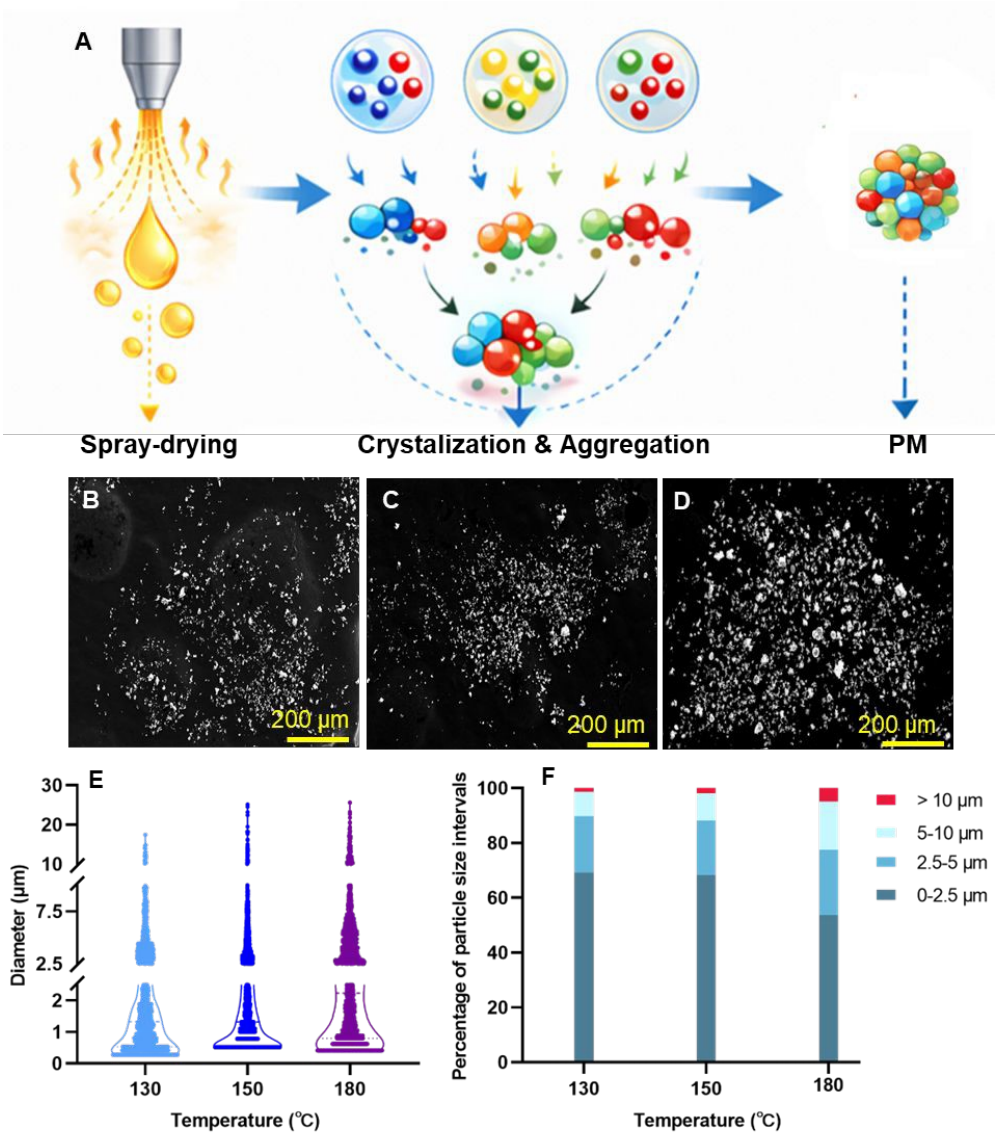

Figure 1. Schematic diagram of spray-drying principle and SEM images of products at different temperatures with statistical results. (A) As the solvent rapidly evaporates, different components undergo crystallization, adsorption, and agglomeration into particles. (B-D) Electron microscope images of particles at different temperatures, from left to right: 130, 150, and 180 °C. (E) Violin plot of particle size distribution. (F) Percentage distribution of particle sizes.

View Article Online
DOI: 10.1039/D6EA00052E

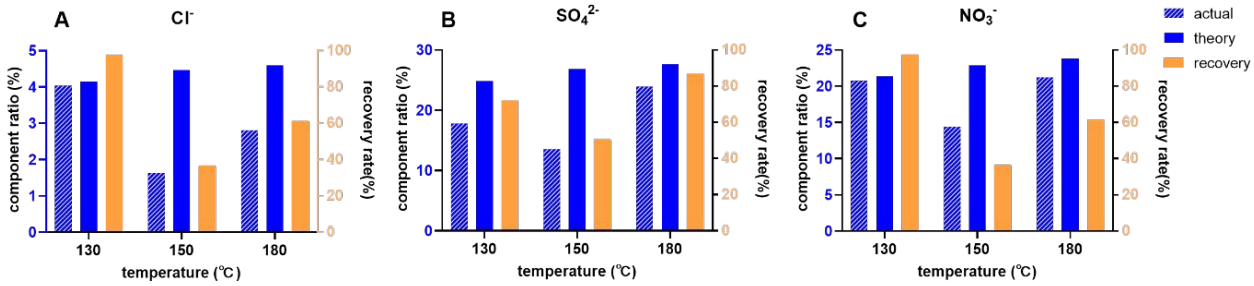

Figure 2. Effect of temperature on recovery rate determined by ion chromatographic method. From left to right: chloride (A), sulfate (B), and nitrate (C).

View Article Online
DOI: 10.1039/D6EA00052E

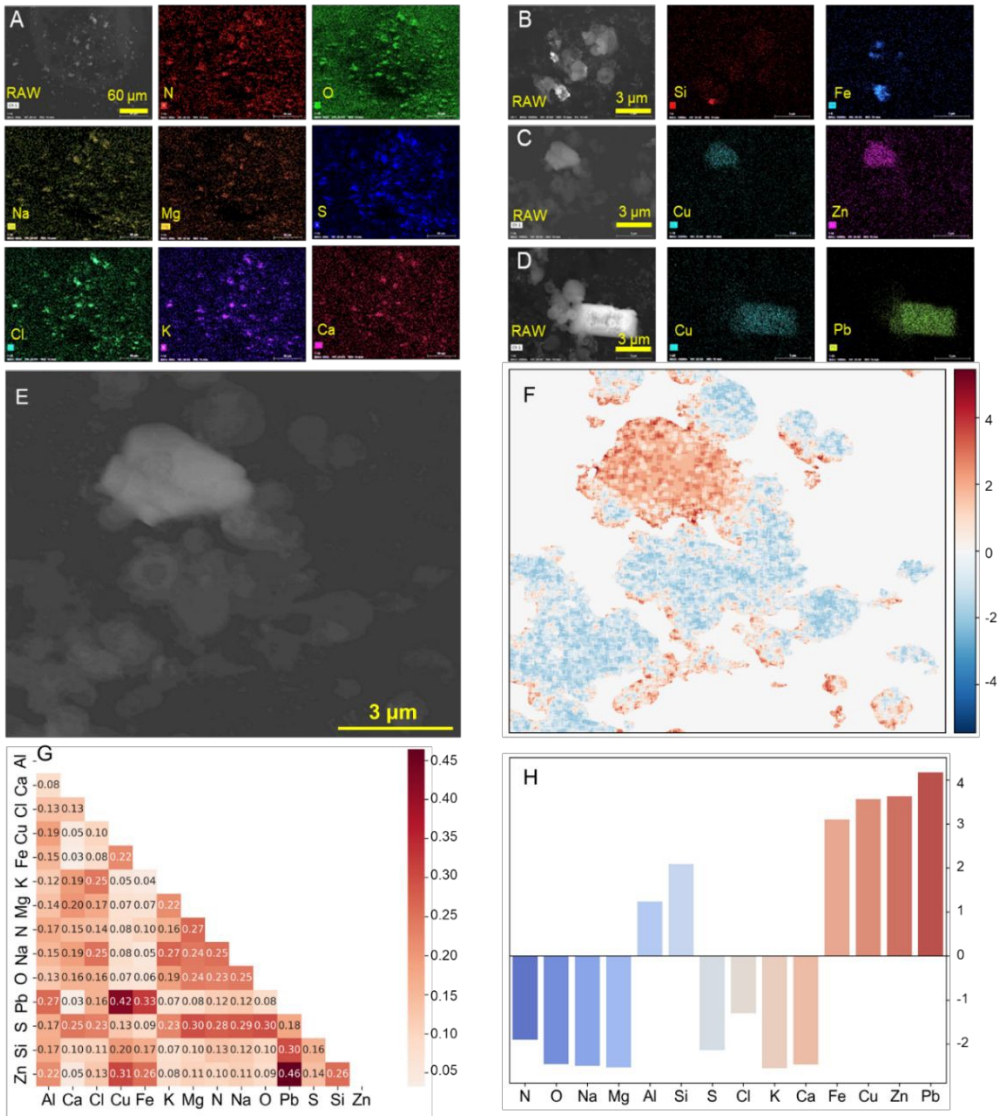

Figure 3. Homogeneous and heterogeneous distribution of different elements. (A) Homogeneous spatial distribution of light elements, including Na, O, Na, Mg, S, Cl, K, and Ca. (B-D) Heterogeneous distribution of elements, including Si, Fe, Cu, Zn, and Pb. (E) A typical electron microscope image revealing the concurrent homogeneous and heterogeneous distribution patterns of elements. (F) Spatial distribution map of elements via principal component analysis (PCA). (G) Heatmap of Spearman's correlation coefficients for each element. (H) PCA loading score plot for each element.

View Article Online
DOI: 10.1039/D6EA00052E

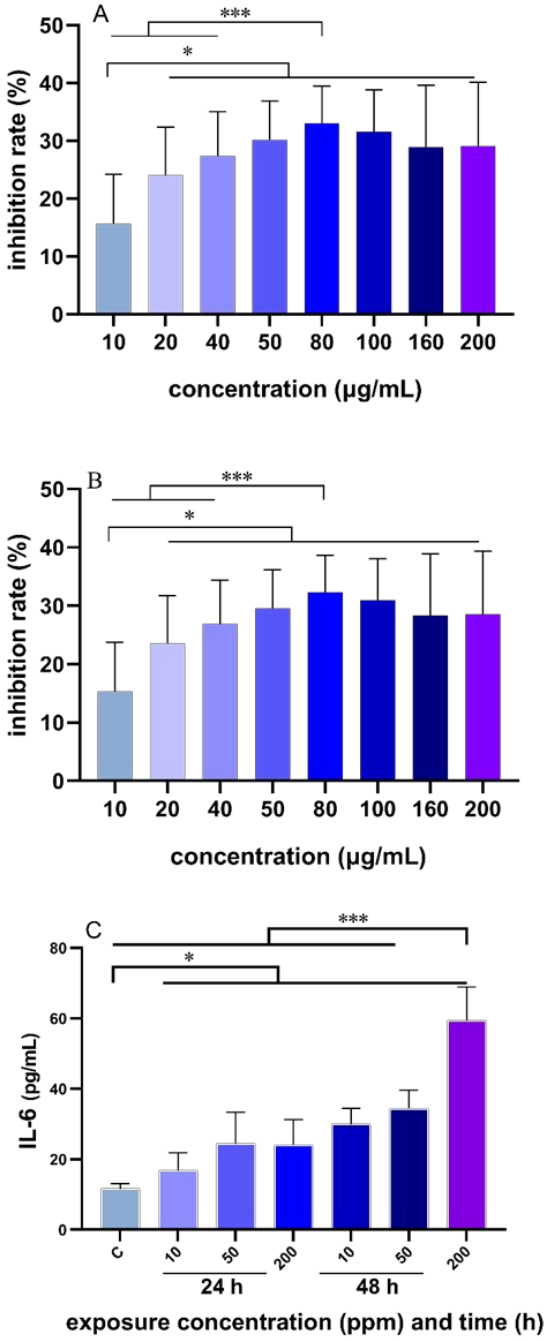

Figure 4. Cycotoxitic results of A549 cells after exposure to synthetic particles. The cell viability of A549 cells at different concentrations after exposure for (A) 24 hours and (B) 48 hours. (C) The level of IL-6 secreted by A549 cells after exposure to synthetic particles at different concentrations and time. Data are shown as mean ± SD, *p* values were given by SPSS software after one-way ANOVA analysis (*: $p<0.05$, ***: $p<0.001$).

View Article Online
DOI: 10.1039/D6EA00052E

Data availability statements

The data supporting this article have been included as part of the Supplementary Information.